Research Article Vol. 31, No. 15 / 17 Jul 2023 / Optics Express 25177
Optics EXPRESS

Optical noise characteristics of injection-locked epitaxial quantum dot lasers on silicon

QI CHU,[1] SHIYUAN ZHAO,[2] JIAWEI WANG,[1] YUNXU SUN,[1] YONG YAO,[1] XIAOCHUAN XU,[1] FRÉDÉRIC GRILLOT,[2,3] AND JIANAN DUAN[1,*]

[1]*State Key Laboratory on Tunable Laser Technology, School of Electronic and Information Engineering, Harbin Institute of Technology, Shenzhen 518055, China*
[2]*LTCI, Telecom Paris, Institut Polytechnique de Paris, 91120 Palaiseau, France*
[3]*Center for High Technology Materials, The University of New-Mexico, Albuquerque, NM 87106, USA*
[*]*duanjianan@hit.edu.cn*

Abstract: This work theoretically investigates the relative intensity noise (RIN) and spectral linewidth characteristics of epitaxial quantum dot (QD) lasers on silicon subject to optical injection. The results show that the RIN of QD lasers can be reduced by optical injection, hence a reduction of 10 dB is achieved which leads to a RIN as low as −167.5 dB/Hz in the stable injection-locked area. Furthermore, the spectral linewidth of the QD laser can be greatly improved through the optical injection locked scheme. It is reduced from 556.5 kHz to 9 kHz with injection ratio of −60 dB and can be further reduced down to 1.5 Hz with injection ratio of 0 dB. This work provides an effective method for designing low intensity noise and ultra-narrow linewidth QD laser sources for photonics integrated circuits on silicon.

1. Introduction

The emergence of 5G, cloud computing, artificial intelligence and coherent optical transceiver modules are driving the development of photonics integrated circuits (PICs) on silicon, which have inherent advantages of CMOS compatibility, high productivity, low-cost manufacturing, high integration density and high energy efficiency [1]. However, due to lattice mismatch, the epitaxial growth of III-V materials on silicon produces a large number of threading dislocation defects (TDD), which act as nonradiative recombination centers in the Shockley-Read-Hall (SRH) process, thereby affecting the performance of lasers [2]. Owing to the high degree of carrier confinement and the atom-like density of states, compared with traditional quantum well (QW) lasers, quantum dot (QD) lasers are more insensitive to the presence of defects [3,4]. Therefore, epitaxial QD lasers on silicon have been regarded as the most potential on-chip laser sources for PICs on silicon [5,6]. The silicon-based QD lasers have recently achieved record performance with long lasing device lifetime [7], near-zero linewidth enhancement factor (α_H) [8], high thermal stability [9] and high feedback resistance [10].

Low optical noise light sources are urgently needed not only for PICs but also for optical transmitters of low-cost data transmission in inter/hyper-data centers and metropolitan data links [11]. The applications such as optical atomic clocks and frequency synthesis also require the low-noise oscillators [12,13]. The optical noise in semiconductor lasers includes relative intensity noise (RIN) and frequency noise (FN), the latter one is usually transformed into spectral linewidth. The RIN reduces the signal-to-noise ratio (SNR) and increases the bit error rate (BER) hence degrading the performance of high-speed optical communication systems and Lidar related applications [14–16]. For QD lasers on native substrate, it has been theoretically and experimentally confirmed that the RIN can be as low as −160 dB/Hz [14,15,17]. However, the presence of TDD can affect the performance of epitaxial QD lasers on silicon or germanium such as limited device lifetime [4], high threshold current [18] and high optical noise [19]. The

#492580 https://doi.org/10.1364/OE.492580
Journal © 2023 Received 10 Apr 2023; revised 14 Jun 2023; accepted 29 Jun 2023; published 14 Jul 2023

Optics EXPRESS

RIN in the range of −120 dB/Hz to −150 dB/Hz has been reported in QD lasers on silicon or germanium [20–22]. Apart from the RIN, the narrow linewidth is also important for high order coherent communications [23,24], optical sensing and metrology [25] as well as free-space optical communication [26]. Owing to the low inversion factor and low α_H factor, spectral linewidth below 100 kHz has been achieved in QD lasers [27]. In order to reach a narrower linewidth, external control schemes such as optical feedback or optical injection are considered as effective methods. By using an external cavity configuration, the spectral linewidth of the QD laser can be reduced to less than 100 kHz [28–30]. However, the precise control of feedback strength is required to make the laser operating in the narrow linewidth area, otherwise the optical feedback will lead to laser instability [31]. It has been shown that the optical injection can considerably improve the dynamical performances of QD lasers including the increase of the modulation bandwidth [32], the decrease of the frequency chirp [33] and the improvement of the frequency comb bandwidth [34]. Optical injection is also an effective method to generate photonic microwave in QD lasers [35,36]. Furthermore, optical injection-locked light sources have been widely used in optical communications and signal processing [37], as well as monolithic PICs [38].

This work theoretically investigates the RIN and spectral linewidth characteristics of epitaxial QD lasers on silicon subject to optical injection. We use the single mode laser model [2], which is more efficient than the multimode approach in dealing with the optical noise [30,39]. The results show that the RIN of the QD laser increases due to the presence of nonradiative recombination process which can be suppressed through optical injection. In the stable injection-locked area, the RIN of the QD laser can be reduced from −157.5 dB/Hz to −167.5 dB/Hz by adjusting the injection ratio and frequency detuning. In addition, the spectral linewidth can be greatly reduced by optical injection, thus the laser linewidth can be decreased to 9 kHz with an injection ratio of −60 dB. Particularly, the ultra-narrow linewidth of 1.5 Hz is achieved with the suppression bandwidth of 28.1 GHz when the injection ratio is 0 dB. This work brings new insights for designing on-chip injection-locked QD lasers on silicon for low noise related applications.

2. Rate equation model of injection-locked QD laser

Figure 1(a) illustrates the schematic representation of an optically injection-locked QD laser system where a tunable laser is used as the master laser and the injected light is coupled into the QD laser (slave laser) through an optical circulator. Figure 1(b) shows the structure of ridged QD laser, whose electronic structure and carrier dynamics in QD active region are depicted in Fig. 1(c). The QD laser exciton model consists of a two-dimensional carrier reservoir (RS), excited state (ES) and ground state (GS). This numerical model assumes that there is only one QD ensemble in the active region, and electrons and holes are considered as neutral excitons. The carriers are firstly captured from the RS into the ES with a capture time τ_{ES}^{RS} and then relax from the ES down to the GS with a relaxation time τ_{GS}^{ES}, and the stimulated emission eventually occurs at GS. Due to the thermalization, carriers are re-emitted from the GS to ES with an escape time τ_{ES}^{GS}, and from the ES to the RS with an escape time τ_{RS}^{ES}, this process is determined by the Fermi distribution of the quasi-equilibrium state. In addition, carriers also recombine spontaneously in each state with spontaneous emission time $\tau_{RS,ES,GS}^{spon}$, respectively. It is necessary to point out that the effect of SRH recombination lifetime τ_{SRH} is considered. Thus, the corpuscular rate equations describing the dynamics of the carrier numbers $N_{RS,ES,GS}$, the photon numbers S_{GS}, and the phase of the electric field ϕ are expressed as:

$$\frac{dN_{RS}}{dt} = \frac{I}{q} + \frac{N_{ES}}{\tau_{RS}^{ES}} - \frac{N_{RS}}{\tau_{ES}^{RS}}(1-\rho_{ES}) - \frac{N_{RS}}{\tau_{RS}^{spon}} - \frac{N_{RS}}{\tau_{SRH}} + F_{RS} \tag{1}$$

Optics EXPRESS

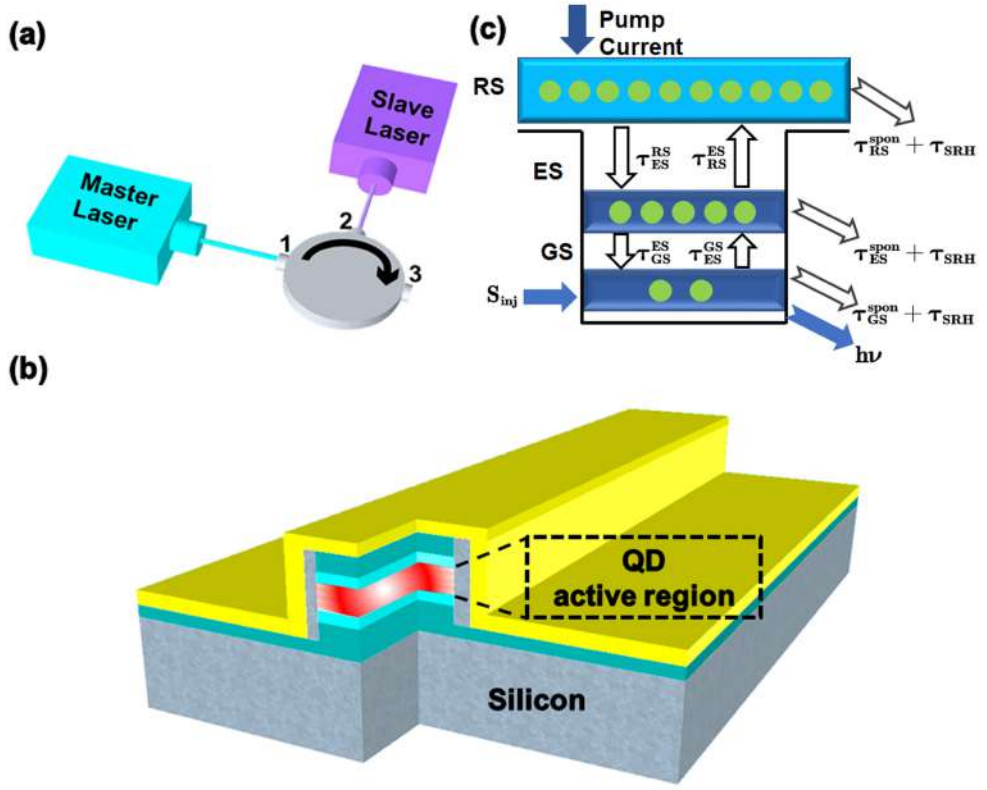

Fig. 1. (a) Schematic representation of an optical injection-locked QD laser system. (b) The structure of epitaxial QD laser on silicon. (c) The electronic structure and carrier dynamics in the QD.

$$\frac{dN_{ES}}{dt} = \left(\frac{N_{RS}}{\tau_{ES}^{RS}} + \frac{N_{GS}}{\tau_{ES}^{GS}}\right)(1-\rho_{ES}) - \frac{N_{ES}}{\tau_{GS}^{ES}}(1-\rho_{GS}) - \frac{N_{ES}}{\tau_{RS}^{ES}} - \frac{N_{ES}}{\tau_{ES}^{spon}} - \frac{N_{ES}}{\tau_{SRH}} + F_{ES} \tag{2}$$

$$\frac{dN_{GS}}{dt} = \frac{N_{ES}}{\tau_{GS}^{ES}}(1-\rho_{GS}) - \frac{N_{GS}}{\tau_{ES}^{GS}}(1-\rho_{ES}) - \Gamma_p v_g g_{GS} S_{GS} - \frac{N_{GS}}{\tau_{GS}^{spon}} - \frac{N_{GS}}{\tau_{SRH}} + F_{GS} \tag{3}$$

$$\frac{dS_{GS}}{dt} = \left(\Gamma_p v_g g_{GS} - \frac{1}{\tau_p}\right) S_{GS} + \beta_{sp}\frac{N_{GS}}{\tau_{GS}^{spon}} + 2k_c\sqrt{S_{inj}S_{GS}}\cos\phi + F_S \tag{4}$$

$$\frac{d\phi}{dt} = \frac{1}{2}\Gamma_p v_g(g_{GS}\alpha_H^{GS} + g_{ES}\alpha_H^{ES} + g_{RS}\alpha_H^{RS}) - \Delta\omega_{inj} - k_c\sqrt{S_{inj}/S_{GS}}\sin\phi + F_\phi \tag{5}$$

where I is the bias current, q is the electron charge, Γ_p is the optical confinement factor, v_g is the group velocity, τ_p is the photon lifetime, β_{sp} is the spontaneous emission factor. The master-slave optical injection mechanism is taken into account with S_{inj} that is the injected photon number from the master laser. The injection ratio is defined as $R_{inj} = S_{inj}/S_0$, where S_0 is the photon number of the solitary laser which means the slave laser is under free-running operation without optical injection. $\Delta\omega_{inj}$ is the frequency detuning defined as the frequency difference between the master laser and the slave laser. k_c is the coupling coefficient of the two lasers, defined as $k_c = v_g(1-R)/(2L\sqrt{R})$ with L being the laser cavity length and R being the facet reflectivity.

Optics EXPRESS

$g_{RS,ES,GS}$ are the material gain of each state:

$$g_{GS} = \frac{a_{GS}}{1 + \epsilon S_{GS}} \frac{N_B}{V_B} (2\rho_{GS} - 1) \tag{6}$$

$$g_{ES} = a_{ES} \frac{N_B}{V_B} (2\rho_{ES} - 1) \tag{7}$$

$$g_{RS} = a_{RS} \frac{D_{RS}}{V_{RS}} (2\rho_{RS} - 1) \tag{8}$$

where $a_{RS,ES,GS}$ are the differential gain, ϵ is the gain compression factor, N_B is the total number of QDs, V_B is the volume of the active region, D_{RS} is the total number of states in the RS, V_{RS} is the volume of the RS, and $\rho_{GS,ES,RS}$ are the carrier occupation probabilities in the GS, ES, and RS, which are given by $\rho_{GS} = \frac{N_{GS}}{2N_B}$, $\rho_{ES} = \frac{N_{ES}}{4N_B}$ and $\rho_{RS} = \frac{N_{RS}}{D_{RS}}$, respectively. $\alpha_H^{RS,ES,GS}$ are the RS, ES, GS contribution to the α_H factor, respectively, and $\alpha_H^{ES,RS}$ are defined by:

$$\alpha_H^{ES,RS} = \frac{\omega_{GS}}{\omega_{ES,RS}} \frac{\left(\omega_{ES,RS} - \omega_{GS}\right) T_D}{1 + \left(\omega_{ES,RS} - \omega_{GS}\right)^2 T_D^2} \tag{9}$$

where T_D is the dephasing time, $\omega_{RS,ES,GS}$ are the angular frequency of each state. $F_{RS,ES,GS}$, F_S, F_ϕ are the Langevin noise for the carrier, photon, and phase noise sources, respectively. The correlation strength of two Langevin noise sources is:

$$\left\langle F_i(t) F_j(t') \right\rangle = U_{i,j} \delta(t - t') \tag{10}$$

where indexes i, j refer to RS, ES, GS, S and ϕ with the diffusion coefficient between two noise sources U_{ij} which are delta-correlated. The diffusion coefficients are expressed as:

$$U_{RSRS} = 2 \times \left(\frac{N_{RS}}{\tau_{ES}^{RS}} (1 - \rho_{ES}) + \frac{N_{RS}}{\tau_{RS}^{spon}} + \frac{N_{RS}}{\tau_{SRH}} \right) \tag{11}$$

$$U_{ESES} = 2 \times \left(\frac{N_{RS}}{\tau_{ES}^{RS}} + \frac{N_{GS}}{\tau_{ES}^{GS}} \right) (1 - \rho_{ES}) \tag{12}$$

$$U_{GSGS} = 2 \times \left[\frac{N_{ES}}{\tau_{GS}^{ES}} (1 - \rho_{GS}) - \Gamma_p v_g g_{GS} S_{GS} + \beta_{sp} \frac{N_{GS}}{\tau_{GS}^{spon}} S_{GS} \right] \tag{13}$$

$$U_{SS} = 2 S_{GS} \left(\beta_{sp} \frac{N_{GS}}{\tau_{GS}^{spon}} - \Gamma_p v_g g_{GS} + \frac{1}{\tau_p} \right) \tag{14}$$

$$U_{\phi\phi} = \frac{1}{2 S_{GS}} \left(\beta_{sp} \frac{N_{GS}}{\tau_{GS}^{spon}} - \Gamma_p v_g g_{GS} + \frac{1}{\tau_p} \right) \tag{15}$$

$$U_{RSES} = - \left[\frac{N_{RS}}{\tau_{ES}^{RS}} (1 - \rho_{ES}) + \frac{N_{ES}}{\tau_{RS}^{ES}} \right] \tag{16}$$

$$U_{ESGS} = - \left[\frac{N_{GS}}{\tau_{ES}^{GS}} (1 - \rho_{ES}) + \frac{N_{ES}}{\tau_{GS}^{ES}} (1 - \rho_{GS}) \right] \tag{17}$$

$$U_{GSS} = - \left[2 \beta_{sp} \frac{N_{GS}}{\tau_{GS}^{spon}} S_{GS} - \Gamma_p v_g g_{GS} S_{GS} \right] \tag{18}$$

Optics EXPRESS

$$U_{RSGS} = U_{RSS} = U_{RS\phi} = U_{ESS} = U_{ES\phi} = U_{GS\phi} = U_{S\phi} = 0 \tag{19}$$

Through a small signal analysis, we linearize the rate Eqs. (1)–(5), and yield:

$$\begin{bmatrix} \gamma_{11}+j\omega & -\gamma_{12} & 0 & 0 & 0 \\ -\gamma_{21} & \gamma_{22}+j\omega & -\gamma_{23} & 0 & 0 \\ 0 & -\gamma_{32} & \gamma_{33}+j\omega & -\gamma_{34} & 0 \\ 0 & 0 & -\gamma_{43} & \gamma_{44}+j\omega & -\gamma_{45} \\ -\gamma_{51} & -\gamma_{52} & -\gamma_{53} & -\gamma_{54} & -\gamma_{55}+j\omega \end{bmatrix} \begin{bmatrix} \delta N_{RS} \\ \delta N_{ES} \\ \delta N_{GS} \\ \delta S_{GS} \\ \delta\phi \end{bmatrix} = \begin{bmatrix} F_{RS} \\ F_{ES} \\ F_{GS} \\ F_S \\ F_\phi \end{bmatrix} \tag{20}$$

with

$$\begin{aligned}
\gamma_{11} &= \frac{1-\rho_{ES}}{\tau_{RS}^{ES}} + \frac{1}{\tau_{RS}^{spon}} + \frac{1}{\tau_{SRH}}, \\
\gamma_{12} &= \frac{1}{\tau_{RS}^{ES}} + \frac{1}{4N_B}\frac{N_{RS}}{\tau_{ES}^{RS}}, \gamma_{21} = \frac{1-\rho_{ES}}{\tau_{RS}^{ES}}, \\
\gamma_{22} &= \frac{1-\rho_{GS}}{\tau_{GS}^{ES}} + \frac{1}{\tau_{RS}^{ES}} + \frac{1}{\tau_{ES}^{spon}} + \frac{1}{4N_B}\left(\frac{N_{RS}}{\tau_{ES}^{RS}} + \frac{N_{GS}}{\tau_{ES}^{GS}}\right) + \frac{1}{\tau_{SRH}}, \\
\gamma_{23} &= \frac{1-\rho_{ES}}{\tau_{ES}^{GS}} + \frac{1}{2N_B}\frac{N_{ES}}{\tau_{GS}^{ES}}, \gamma_{32} = \frac{1-\rho_{GS}}{\tau_{GS}^{ES}} + \frac{1}{4N_B}\frac{N_{GS}}{\tau_{ES}^{GS}}, \\
\gamma_{33} &= \frac{1-\rho_{ES}}{\tau_{ES}^{GS}} + \frac{1}{2N_B}\frac{N_{ES}}{\tau_{GS}^{ES}} + \frac{1}{\tau_{GS}^{spon}} + \frac{1}{\tau_{SRH}} + \Gamma_p v_g a S_{GS}, \\
\gamma_{34} &= -\Gamma_p v_g g_{GS} + \Gamma_p v_g a_p S_{GS}, \gamma_{43} = \Gamma_p v_g a S_{GS} + \frac{\beta_{sp}}{\tau_{GS}^{spon}}, \\
\gamma_{44} &= \frac{1}{\tau_p} - \Gamma_p v_g g_{GS} + \Gamma_p v_g a_p S_{GS} - k_c \cos\phi\sqrt{S_{inj}/S_{GS}}, \\
\gamma_{45} &= -2k_c \sin\phi\sqrt{S_{inj}S_{GS}}, \gamma_{51} = \Gamma_p v_g a_{RS}\alpha_H^{RS}, \\
\gamma_{52} &= \frac{1}{4}\Gamma_p v_g a_{ES}\alpha_H^{ES}, \gamma_{53} = \frac{1}{2}\Gamma_p v_g a \alpha_H^{GS}, \\
\gamma_{54} &= -\frac{1}{2}\Gamma_p v_g a_p \alpha_H^{GS} + \frac{k_c}{2S_{GS}}\sqrt{S_{inj}/S_{GS}}\sin\phi, \\
\gamma_{55} &= k_c \cos\phi\sqrt{S_{inj}/S_{GS}}
\end{aligned} \tag{21}$$

where a and a_p take into account the gain compression at high photon numbers such as $dg_{GS} = ad_{GS} - a_p dS_{GS}$. Following the Cramer's rule, the RIN and FN of the QD laser are expressed as follows:

$$RIN(\omega) = \left|\frac{\delta S_{GS}(\omega)}{S_{GS}}\right|^2 \tag{22}$$

$$FN(\omega) = \left|\frac{j\omega}{2\pi}\delta\phi(\omega)\right|^2 \tag{23}$$

with $\delta S_{GS}(\omega)$ and $\delta\phi(\omega)$ being the photon number and phase variation in the frequency domain. S_{GS} is the steady state photon number. The spectral linewidth $\Delta\nu_{SL}$ of the QD laser is extracted from the FN spectrum at 1 MHz and can be expressed as [14]:

$$\Delta\nu_{SL} = \Delta\nu_{IL}(1+\alpha_H^2) \tag{24}$$

where $\Delta\nu_{IL}$ is intrinsic linewidth determined only by spontaneous emission. By contrast, the $\Delta\nu_{SL}$ is determined not only by spontaneous emission, but also by carrier fluctuations through the

Optics EXPRESS

phase-amplitude coupling effect (α_H). All material and optical parameters used in the simulation are listed in Table 1 unless stated otherwise [2].

Table 1. Material and optical parameters of the QD laser.

Symbol	Description	Value
E_{RS}	RS energy level	0.97 eV
E_{ES}	ES energy level	0.87 eV
E_{GS}	GS energy level	0.82 eV
τ_{ES}^{RS}	RS to ES capture time	6.3 ps
τ_{GS}^{ES}	ES to GS relaxation time	2.9 ps
τ_{RS}^{ES}	ES to RS escape time	2.7 ns
τ_{ES}^{GS}	GS to ES escape time	10.4 ps
τ_{RS}^{spon}	RS spontaneous emission lifetime	0.5 ns
τ_{ES}^{spon}	ES spontaneous emission lifetime	0.5 ns
τ_{GS}^{spon}	GS spontaneous emission lifetime	1.2 ns
τ_p	Photon lifetime	4.1 ps
T_D	Polarization dephasing time	0.1 ps
τ_{SRH}	Nonradiative recombination lifetime	0.5 - 10 ns (*variable*)
β_{sp}	Spontaneous emission factor	1.0×10^{-4}
ϵ	Gain compression factor	2.0×10^{-16} cm^3
Γ_p	Optical confinement factor	0.06
a_{GS}	GS Differential gain	5.0×10^{-15} cm^2
a_{ES}	ES Differential gain	10×10^{-15} cm^2
a_{RS}	RS Differential gain	2.5×10^{-15} cm^2
α_H^{GS}	GS contribution to α_H-factor	0.50
N_B	Total dot number	1.0×10^7
D_{RS}	Total RS state number	4.8×10^6
V_B	The volume of active region	5.0×10^{-11} cm^3
V_{RS}	The volume of RS region	1.0×10^{-11} cm^3
k_c	Injection coupling coefficient	10×10^{10} s^{-1}

3. Result and discussion

3.1. Nonradiative recombination effect

The epitaxial defect density of QD laser on native substrate is typically in the range of 10^3 - 10^4 cm^{-2} which corresponds to τ_{SRH} on the order larger than 10 ns. For silicon-based QD lasers where the defect density is at least two orders of magnitude higher than that in QD lasers on native substrate hence the τ_{SRH} is less than 10 ns [2]. The explored range of τ_{SRH} in QD lasers on silicon is from 0.5 ns to 10 ns, which correspond to the defect density from 1.3×10^6 cm^{-2} to 1.3×10^8 cm^{-2}. Figure 2(a) depicts the photon number as a function of the bias current for different τ_{SRH} ranging from 0.5 ns to 10 ns. The threshold current increases from 52 mA at τ_{SRH} = 10 ns to 125 mA at τ_{SRH} = 0.5 ns due to the high defect density [18]. As the threshold current changes with the variation of the τ_{SRH}, for fair comparison, the photon number of solitary laser is fixed (3×10^5) for different τ_{SRH} in the optical noise simulations rather than the bias currents due to the fact that the optical noise is closely related to the photon number. Figure 2(b) depicts the RIN spectra of QD laser for different τ_{SRH}. The low frequency RIN level below the relaxation

Optics EXPRESS

oscillation frequency (ROF) is increased with a short τ_{SRH} due to the shorten carrier lifetime. The RIN at 10 MHz increases from −161 dB/Hz at τ_{SRH} = 10 ns to −157.5 dB/Hz at τ_{SRH} = 0.5 ns while the RIN above the ROF remains unchanged. Figure 2(c) shows the FN spectra for different τ_{SRH} which exhibit a high resonance peak in the frequency range of 1∼10 GHz due to the QD laser is under-damped [40]. The FN maintains stable for different τ_{SRH} in the whole frequency range except the resonance peak. The spectral linewidth of QD laser is 556.5 kHz at τ_{SRH} = 0.5 ns, which is extracted from the FN spectrum at 1 MHz. Figure 2(d) demonstrates the effect of nonradiative recombination on the modulation response through small signal analysis and the corresponding 3 dB modulation bandwidth are shown in the inset of Fig. 2(d). The fast nonradiative recombination shortens the total carrier lifetime, hence significantly enhancing the damping factor and suppressing the resonance peak, which lead to the limited 3 dB modulation bandwidth [19].

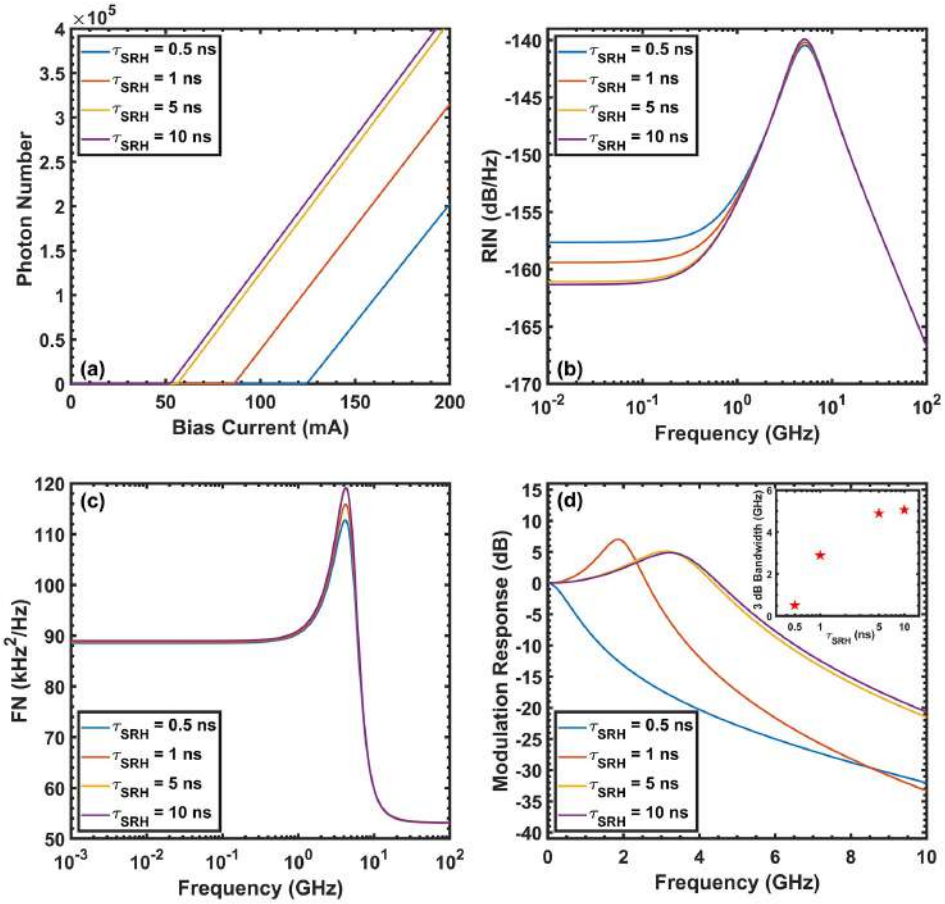

Fig. 2. Nonradiative recombination effect on the (a) light-current characteristics, (b) RIN spectra, (c) FN spectra and (d) modulation response. The inset exhibits the nonradiative recombination effect on the 3 dB modulation bandwidth.

Optics EXPRESS

3.2. Optical injection effect on the modulation dynamics

The effect of optical injection on the modulation dynamics is now investigated through the small signal analysis. The modulation transfer function of QD laser is expressed as [41] :

$$H(\omega) = \frac{R_0}{\Delta} = \frac{R_0}{R_0 + j\omega R_1 - \omega^2 R_2 - j\omega^3 R_3 + \omega^4} \tag{25}$$

where Δ is the determinant of the matrix in Eq. (20) except the phase equation. The four parameters that characterize the $H(\omega)$ are defined by:

$$\begin{aligned} R_0 &= \omega_R^2 \omega_{R0}^2 - \gamma_{23}\gamma_{44}(\gamma_{11}\gamma_{32} + \gamma_{12}\gamma_{31}) \\ R_1 &= \omega_R^2 \Gamma_0 + \omega_{R0}^2 \Gamma - \gamma_{23}\gamma_{32}(\gamma_{11} + \gamma_{44}) - \gamma_{12}\gamma_{23}\gamma_{31} \\ R_2 &= \omega_R^2 + \Gamma_0\Gamma + \omega_{R0}^2 - \gamma_{23}\gamma_{32} \\ R_3 &= \Gamma_0 + \Gamma \end{aligned}$$

with ω_R is the ROF and γ is the damping factor. Figure 3(a) shows the modulation response of the injection-locked QD laser operating near the threshold current for different injection ratios at zero frequency detuning. Compared with the solitary case, the peak of the ROF is suppressed when the laser is stable locked [42]. Figure 3(b) depicts the corresponding 3 dB modulation bandwidth as a function of the optical injection ratio. The 3 dB bandwidth of the QD laser increases from 0.6 GHz in the solitary case to 3 GHz at $R_{inj} = 4$ since the large injection ratio increases the damping factor hence allowing the laser shows a broadband and flat response [40]. This indicates that the modulation dynamics of QD lasers can be greatly improved through optical injection.

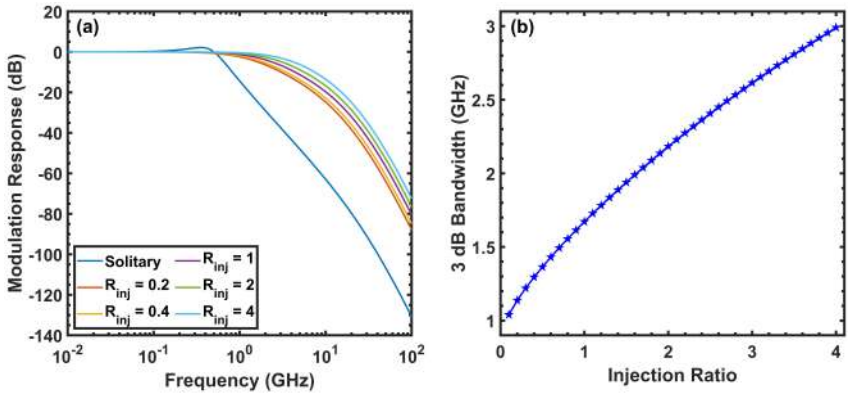

Fig. 3. Optical injection ratio dependence of (a) the modulation response and (b) the 3 dB modulation bandwidth with $\tau_{SRH} = 10$ ns at zero frequency detuning.

3.3. Optical injection effect on the RIN

The effect of optical injection ratio on the RIN performance of QD laser is investigated. Figure 4(a) compares the RIN spectra in the solitary case and for different injection ratios at zero frequency detuning with $\tau_{SRH} = 10$ ns. The RIN level decreases in the whole spectral range with the increase of the injection ratio while the ROF shifts towards a higher frequency along with a reduced peak amplitude. This tendency is consistent with the previous modulation response because the modulation properties and the noise spectra are driven by the same dynamical processes in QD lasers [21]. Particularly, the low-frequency RIN at 10 MHz decreases from -161 dB/Hz for solitary case down to -167 dB/Hz with $R_{inj} = 4$. The injection ratio dependence

Optics EXPRESS

of low-frequency RIN versus τ_{SRH} from 0.5 ns to 10 ns is shown in the Fig. 4(b). Compared with the solitary case, the RIN in the injection-locked area is reduced by about 6 dB at τ_{SRH} = 10 ns, and 10 dB at τ_{SRH} = 0.5 ns with R_{inj} = 4. In addition, it is noted that the RIN is almost constant at −167.5 dB/Hz for different nonradiative recombination lifetime when further increasing the injection ratio, hence the effect of nonradiative recombination on the RIN can be completely offset through the optical injection in silicon-based QD lasers.

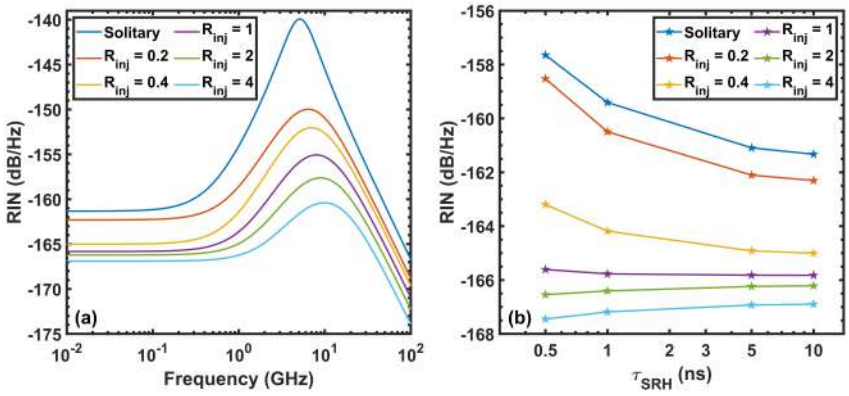

Fig. 4. (a) Injection ratio dependence of the RIN spectra with τ_{SRH} = 10 ns at zero frequency detuning. (b) Low-frequency RIN at 0.01 GHz versus τ_{SRH} for different injection ratio at zero frequency detuning.

The effect of frequency detuning on the RIN is analysed through the optical injection mapping. The stable optical injection-locked area of QD laser is determined by analysing the time series of the photon number subject to optical injection [43]. The time series of the photon number in the stable area converges at a certain constant as shown in the Fig. 5(a), while that in the unstable area is always fluctuating (Fig. 5(b)). Figure 5(c) demonstrates the boundaries of the stable injection-locked area for different nonradiative recombination lifetime. The boundary curves of the stable locked area corresponding to different τ_{SRH} are almost coincident, hence the SRH process has little impact on the stable locked area of QD lasers. The high density defects induced SRH process shortens the carrier lifetime and enhance the damping factor of the slave laser, without greatly affecting the coupling between the master and slave lasers.

Figure 6(a) and (b) display the mapping of the RIN with the variation of both injection ratio and frequency detuning at τ_{SRH} = 10 ns and τ_{SRH} = 0.5 ns, respectively. In the stable injection-locked area, the RIN is reduced down to −167.5 dB/Hz with the increase of the injection ratio and frequency detuning. The boundaries of stable injection-locked area of RIN keep at the same level for different nonradiative recombination lifetime, which is also confirmed by the Fig. 5(c). However, this stable area is asymmetric with respect to zero frequency detuning and shifts to positive frequency detuning which can be attributed to the asymmetry in the gain profile leading to a non-zero α_H factor that is fixed at 0.5. Figure 6(c) and (d) depict the mapping of the RIN at α_H = 1 and α_H = 2, indicating that the stable locked area is strongly dependent on the α_H. The stable injection-locked area moves in the direction of large injection ratio and frequency detuning with the increase of the α_H. In addition, the gain peak α_H is lower at short wavelength than that of long wavelength, hence the negative detuning region is more chaotic than the positive detuning region [44,45].

3.4. Optical injection effect on the spectral linewidth

The effect of optical injection on the FN and spectral linewidth performance of QD laser is now investigated. It is found that a very low injection ratio can greatly reduce the spectral linewidth

Optics EXPRESS

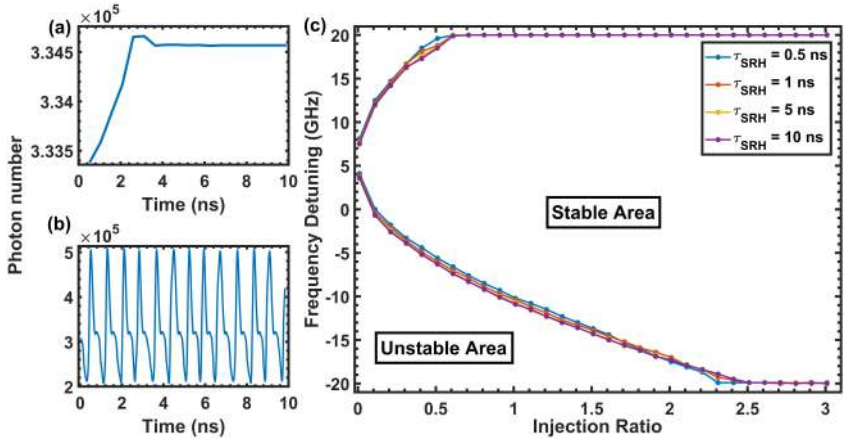

Fig. 5. Time series of photon numbers in the (a) stable and (b) unstable area. (c) Stable locked boundaries of QD laser for different nonradiative recombination lifetime.

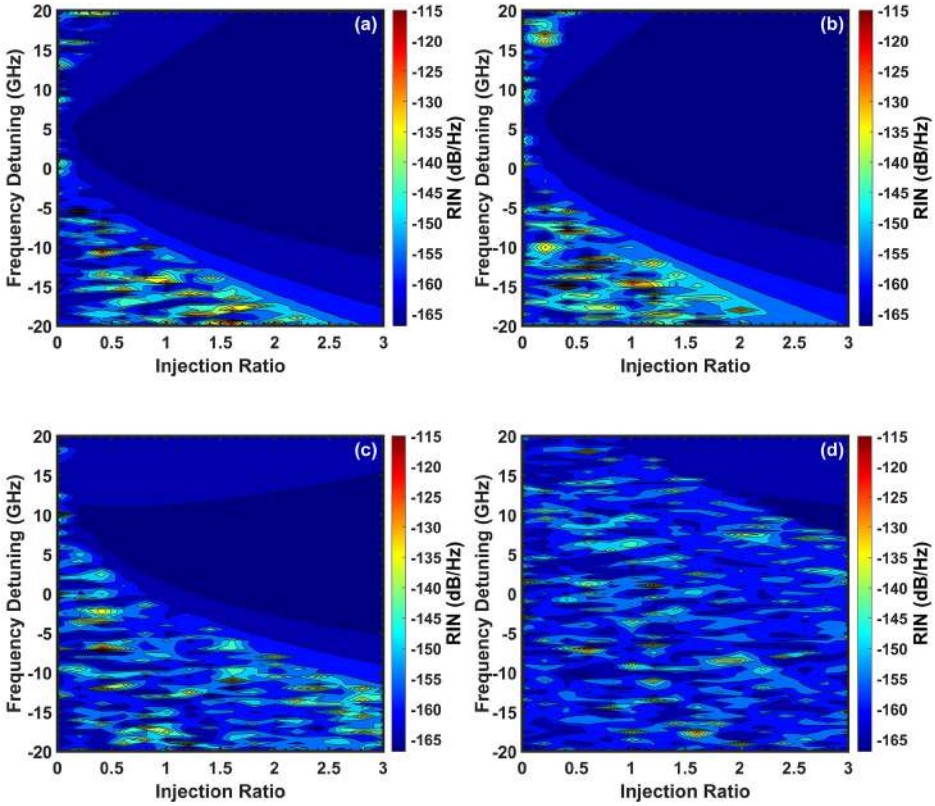

Fig. 6. The mapping of the RIN with the variation of injection ratio and frequency detuning for (a) $\tau_{SRH} = 10$ ns and (b) $\tau_{SRH} = 0.5$ ns. The mapping of the RIN with $\tau_{SRH} = 10$ ns for (c) $\alpha_H = 1$ and (d) $\alpha_H = 2$.

of the laser hence the injection ratio is converted to dB in this section. Figure 7(a) presents the FN spectra of the injection-locked QD laser for different injection ratios with $\tau_{SRH} = 0.5$ ns and at zero frequency detuning. The low-frequency FN below the resonance peak is significantly

Optics EXPRESS

reduced with optical injection which is due to the strong locking of the low-frequency phase between the slave laser and the master laser. Also, the FN under optical injection exhibits a wider resonance peak than the solitary laser, which is caused by carrier noise disturbance [46]. Figure 7(b) reveals the spectral linewidth extracted from the low-frequency FN at 1 MHz versus the injection ratio for different nonradiative recombination lifetime. For silicon-based QD lasers with τ_{SRH} = 0.5 ns, the spectral linewidth is dramatically decreased from 556.5 kHz to 9 kHz for a low injection ratio of −60 dB. When the injection ratio is greater than −10 dB, the entire FN spectrum is completely suppressed and the linewidth is reduced down to 1.5 Hz for injection ratio of 0 dB. In addition, the spectral linewidth decreases at a fixed injection ratio as the nonradiative recombination lifetime increases. It is noted that the spectral linewidth of the injection locked QD laser is controlled only by the FN of the master laser, and no longer follows the intrinsic limit of the laser [43].

The suppression bandwidth is defined as the bandwidth of FN subject to optical injection which is lower than −3 dB of the FN for solitary laser. Therefore, the FN below the suppression bandwidth is mainly determined by the master laser, while that above the bandwidth is mainly determined by the slave laser [43]. Figure 8(a) and (b) demonstrate the mapping of the FN suppression bandwidth with the variation of both injection ratio and frequency detuning for

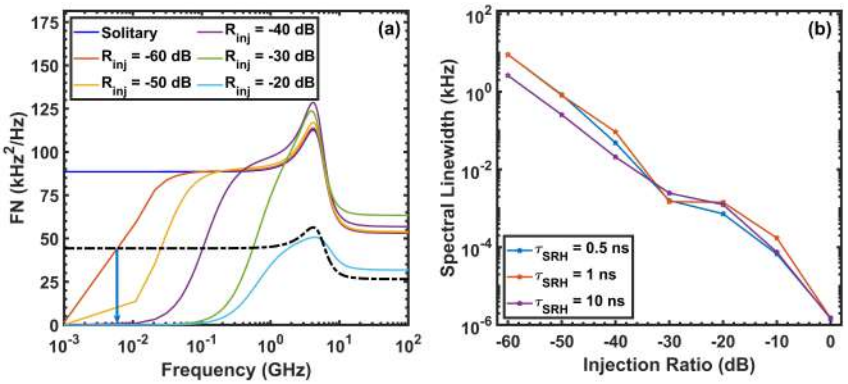

Fig. 7. (a) Injection ratio dependence of the FN spectra with τ_{SRH} = 0.5 ns. (The dashed line represents the −3 dB of the FN for solitary laser.) (b) Spectral linewidth versus injection ratio for different nonradiative recombination lifetime.

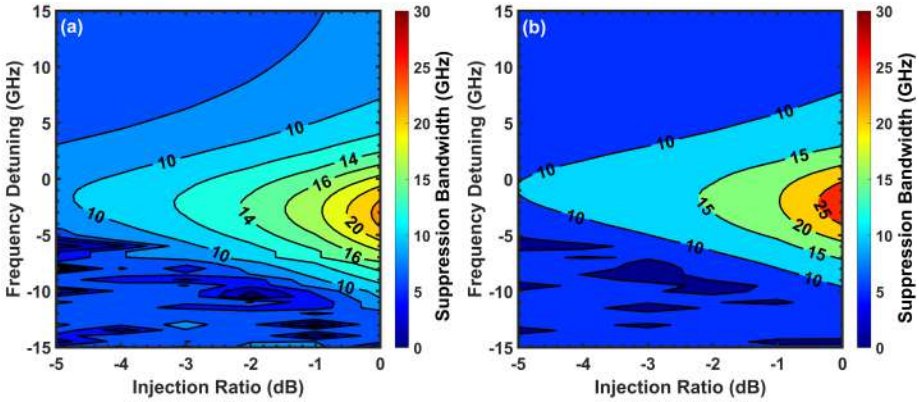

Fig. 8. The suppression bandwidth with the variation of injection ratio and frequency detuning for (a) τ_{SRH} = 10 ns, (b) τ_{SRH} = 0.5 ns.

Optics EXPRESS

τ_{SRH} = 10 ns and τ_{SRH} = 0.5 ns, respectively. The suppression bandwidth increases with the increase of the injection ratio near the zero frequency detuning, while the maximum values are obtained on the negative detuning side. For a strong injection ratio of 0 dB, the maximum suppression bandwidth is 22.7 GHz for τ_{SRH} = 10 ns and is further enhanced to 28.1 GHz for τ_{SRH} = 0.5 ns, indicating that narrow spectral linewidth can be achieved in silicon-based QD lasers by optical injection. In addition, compared the Fig. 8 with the Fig. 6, in the low injection ratio regime, the stable injection-locked area of the FN is more symmetric than that of the RIN with respect to zero frequency detuning.

4. Conclusion

In this paper, we theoretically investigate the effect of optical injection on the optical noise properties of epitaxial QD lasers on silicon considering the presence of SRH recombination. The high defect density in silicon-based QD lasers shortens the SRH lifetime, hence increasing the optical noise and degrading the modulation bandwidth. These results demonstrate that the 3 dB modulation bandwidth, the RIN and the spectral linewidth are greatly improved in epitaxial QD lasers on silicon through the optical injection, and the effect of SRH can be offset by optical injection. The optical injection has been confirmed to reduce the α_H and enhance the damping factor [33]. Theorefore, the RIN down to −167.5 dB/Hz is realized with a reduction of 10 dB through optical injection, hence the tolerance to high defect density of 10^8 cm^{-2} is achieved. The optical injection can also significantly reduce the spectral linewidth from the order of kHz to the order of Hz along with a suppression bandwidth of 28.1 GHz. Overall, this work confirms that optical injection is an effective method for achieving low-noise and narrow linewidth epitaxial QD lasers on silicon, which are meaningful for PICs on silicon.

Funding. National Key Research and Development Program of China (2022YFB2803600); National Natural Science Foundation of China (62105080, 62204072, U22A2093); Basic and Applied Basic Research Foundation of Guangdong Province (2020A1515110328, 2021A1515110076, 2023A1515012304); Shenzhen Science and Technology Innovation Program (GXWD20220811163623002, RCBS20210609103824050).

Acknowledgement. Authors acknowledge Dr. Xingguang Wang and Porf. Cheng Wang from ShanghaiTech University, Shanghai, China for fruitful discussions.

Disclosures. The authors declare no conflicts of interest.

Data availability. Data underlying the results presented in this paper are not publicly available at this time but may be obtained from the authors upon reasonable request.

References

1. C. Xiang, W. Jin, D. Huang, M. A. Tran, J. Guo, Y. Wan, W. Xie, G. Kurczveil, A. M. Netherton, D. Liang, H. Rong, and J. E. Bowers, "High-performance silicon photonics using heterogeneous integration," IEEE J. Sel. Top. Quantum Electron. **28**(3), 1–15 (2022).
2. S. Zhao and F. Grillot, "Effect of shockley-read-hall recombination on the static and dynamical characteristics of epitaxial quantum-dot lasers on silicon," Phys. Rev. A **103**(6), 063521 (2021).
3. R. Beanland, A. Sánchez, D. Childs, K. Groom, H. Liu, D. Mowbray, and M. Hopkinson, "Structural analysis of life tested 1.3 μm quantum dot lasers," J. Appl. Phys. **103**(1), 014913 (2008).
4. J. Liu, M. Tang, H. Deng, S. Shutts, L. Wang, P. M. Smowton, C. Jin, S. Chen, A. Seeds, and H. Liu, "Theoretical analysis and modelling of degradation for III–V lasers on si," J. Phys. D: Appl. Phys. **55**(40), 404006 (2022).
5. J. C. Norman, D. Jung, Y. Wan, and J. E. Bowers, "Perspective: The future of quantum dot photonic integrated circuits," APL Photonics **3**(3), 030901 (2018).
6. J. Duan, H. Huang, B. Dong, D. Jung, J. C. Norman, J. E. Bowers, and F. Grillot, "1.3-μm reflection insensitive InAs/GaAs quantum dot lasers directly grown on silicon," IEEE Photonics Technol. Lett. **31**(5), 345–348 (2019).
7. J. C. Norman, D. Jung, Z. Zhang, Y. Wan, S. Liu, C. Shang, R. W. Herrick, W. W. Chow, A. C. Gossard, and J. E. Bowers, "A review of high-performance quantum dot lasers on silicon," IEEE J. Quantum Electron. **55**(2), 1–11 (2019).
8. J. Duan, H. Huang, B. Dong, J. C. Norman, Z. Zhang, J. E. Bowers, and F. Grillot, "Dynamic and nonlinear properties of epitaxial quantum dot lasers on silicon for isolator-free integration," Photonics Res. **7**(11), 1222–1228 (2019).
9. K. Nishi, K. Takemasa, M. Sugawara, and Y. Arakawa, "Development of quantum dot lasers for data-com and silicon photonics applications," IEEE J. Sel. Top. Quantum Electron. **23**(6), 1–7 (2017).

Optics EXPRESS

10. J. Duan, Y. Zhou, H. Huang, B. Dong, C. Wang, and F. Grillot, "Dynamic properties of two-state lasing quantum dot laser for external optical feedback resistant applications," in *2020 International Conference on Numerical Simulation of Optoelectronic Devices (NUSOD)* (IEEE, 2020), pp. 79–80.
11. M. Liao, S. Chen, Z. Liu, Y. Wang, L. Ponnampalam, Z. Zhou, J. Wu, M. Tang, S. Shutts, Z. Liu, P. M. Smowton, S. Yu, A. Seeds, and H. Liu, "Low-noise 1.3 μm InAs/GaAs quantum dot laser monolithically grown on silicon," Photonics Res. **6**(11), 1062–1066 (2018).
12. D. T. Spencer, T. Drake, and T. C. Briles, *et al.*, "An optical-frequency synthesizer using integrated photonics," Nature **557**(7703), 81–85 (2018).
13. F. Grillot, J. Duan, B. Dong, and H. Huang, "Uncovering recent progress in nanostructured light-emitters for information and communication technologies," Light: Sci. Appl. **10**(1), 156 (2021).
14. J. Duan, X.-G. Wang, Y.-G. Zhou, C. Wang, and F. Grillot, "Carrier-noise-enhanced relative intensity noise of quantum dot lasers," IEEE J. Quantum Electron. **54**(6), 1–7 (2018).
15. Y. Zhou, J. Duan, F. Grillot, and C. Wang, "Optical noise of dual-state lasing quantum dot lasers," IEEE J. Quantum Electron. **56**(6), 1–7 (2020).
16. C. H. Cox, E. I. Ackerman, G. E. Betts, and J. L. Prince, "Limits on the performance of rf-over-fiber links and their impact on device design," IEEE Trans. Microwave Theory Tech. **54**(2), 906–920 (2006).
17. A. Capua, L. Rozenfeld, V. Mikhelashvili, G. Eisenstein, M. Kuntz, M. Laemmlin, and D. Bimberg, "Direct correlation between a highly damped modulation response and ultra low relative intensity noise in an InAs/GaAs quantum dot laser," Opt. Express **15**(9), 5388–5393 (2007).
18. M. Buffolo, L. Rovere, C. De Santi, D. Jung, J. Norman, J. E. Bowers, R. W. Herrick, G. Meneghesso, E. Zanoni, and M. Meneghini, "Degradation of 1.3 μm InAs quantum-dot laser diodes: Impact of dislocation density and number of quantum dot layers," IEEE J. Quantum Electron. **57**(1), 1–8 (2021).
19. C. Wang and Y. Zhou, "Dynamics of InAs/GaAs quantum dot lasers epitaxially grown on Ge or Si substrate," J. Semicond. **40**(10), 101306 (2019).
20. Y.-G. Zhou, C. Zhou, C.-F. Cao, J.-B. Du, Q. Gong, and C. Wang, "Relative intensity noise of InAs quantum dot lasers epitaxially grown on Ge," Opt. Express **25**(23), 28817–28824 (2017).
21. J. Duan, Y. Zhou, B. Dong, H. Huang, J. C. Norman, D. Jung, Z. Zhang, C. Wang, J. E. Bowers, and F. Grillot, "Effect of p-doping on the intensity noise of epitaxial quantum dot lasers on silicon," Opt. Lett. **45**(17), 4887–4890 (2020).
22. A. Y. Liu, T. Komljenovic, M. L. Davenport, A. C. Gossard, and J. E. Bowers, "Reflection sensitivity of 1.3 μm quantum dot lasers epitaxially grown on silicon," Opt. Express **25**(9), 9535–9543 (2017).
23. Z. Zhang, K. Zou, H. Wang, P. Liao, N. Satyan, G. Rakuljic, A. E. Willner, and A. Yariv, "High-speed coherent optical communication with isolator-free heterogeneous Si/III-V lasers," J. Lightwave Technol. **38**(23), 6584–6590 (2020).
24. M. Seimetz, "Laser linewidth limitations for optical systems with high-order modulation employing feed forward digital carrier phase estimation," in *optical fiber communication conference*, (Optical Society of America, 2008), p. OTuM2.
25. M. A. Tran, D. Huang, and J. E. Bowers, "Tutorial on narrow linewidth tunable semiconductor lasers using Si/III-V heterogeneous integration," APL Photonics **4**(11), 111101 (2019).
26. M. Chi, O. B. Jensen, J. Holm, C. Pedersen, P. E. Andersen, G. Erbert, B. Sumpf, and P. M. Petersen, "Tunable high-power narrow-linewidth semiconductor laser based on an external-cavity tapered amplifier," Opt. Express **13**(26), 10589–10596 (2005).
27. J. Duan, H. Huang, Z. Lu, P. Poole, C. Wang, and F. Grillot, "Narrow spectral linewidth in InAs/InP quantum dot distributed feedback lasers," Appl. Phys. Lett. **112**(12), 121102 (2018).
28. A. Y. Nevsky, U. Bressel, I. Ernsting, C. Eisele, M. Okhapkin, S. Schiller, A. Gubenko, D. Livshits, S. Mikhrin, I. Krestnikov, and A. Kovsh, "A narrow-line-width external cavity quantum dot laser for high-resolution spectroscopy in the near-infrared and yellow spectral ranges," Appl. Phys. B **92**(4), 501–507 (2008).
29. J. F. Ehlert, A. Mugnier, G. He, and F. Grillot, "Modeling of a quantum dot gain chip in an external cavity laser configuration," Laser Phys. **31**(8), 085002 (2021).
30. W. W. Chow, Y. Wan, J. E. Bowers, and F. Grillot, "Analysis of the spontaneous emission limited linewidth of an integrated III–V/SiN laser," Laser Photonics Rev. **16**(6), 2100620 (2022).
31. L. A. Coldren, S. W. Corzine, and M. L. Mashanovitch, *Diode lasers and photonic integrated circuits* (John Wiley Sons, 2012).
32. T. Erneux, E. Viktorov, B. Kelleher, D. Goulding, S. Hegarty, and G. Huyet, "Optically injected quantum-dot lasers," Opt. Lett. **35**(7), 937–939 (2010).
33. C. Wang, M. E. Chaibi, H. Huang, D. Erasme, P. Poole, J. Even, and F. Grillot, "Frequency-dependent linewidth enhancement factor of optical injection-locked quantum dot/dash lasers," Opt. Express **23**(17), 21761–21770 (2015).
34. B. Dong, H. Huang, J. Duan, G. Kurczveil, D. Liang, R. G. Beausoleil, and F. Grillot, "Frequency comb dynamics of a 1.3 μm hybrid-silicon quantum dot semiconductor laser with optical injection," Opt. Lett. **44**(23), 5755–5758 (2019).
35. C. Wang, R. Raghunathan, K. Schires, S.-C. Chan, L. F. Lester, and F. Grillot, "Optically injected InAs/GaAs quantum dot laser for tunable photonic microwave generation," Opt. Lett. **41**(6), 1153–1156 (2016).

Optics EXPRESS

36. Z.-F. Jiang, Z.-M. Wu, E. Jayaprasath, W.-Y. Yang, C.-X. Hu, and G.-Q. Xia, "Nonlinear dynamics of exclusive excited-state emission quantum dot lasers under optical injection, in Photonics, vol. 6 (MDPI, 2019), p. 58.," IEEE J. Sel. Top. Quantum Electron. **28**(1: Semiconductor Lasers), 1–12 (2022).
37. Z. Liu and R. Slavík, "Optical injection locking: From principle to applications," J. Lightwave Technol. **38**(1), 43–59 (2020).
38. K. Balakier, M. J. Fice, F. van Dijk, G. Kervella, G. Carpintero, A. J. Seeds, and C. C. Renaud, "Optical injection locking of monolithically integrated photonic source for generation of high purity signals above 100 GHz," Opt. Express **22**(24), 29404–29412 (2014).
39. M. Saldutti, A. Tibaldi, F. Cappelluti, and M. Gioannini, "Impact of carrier transport on the performance of QD lasers on silicon: a drift-diffusion approach," Photonics Res. **8**(8), 1388–1397 (2020).
40. C. Wang, "Modulation dynamics of InP-based quantum dot lasers and quantum cascade lasers," Ph.D. thesis, INSA de Rennes (2015).
41. C. Wang, F. Grillot, and J. Even, "Impacts of wetting layer and excited state on the modulation response of quantum-dot lasers," IEEE J. Quantum Electron. **48**(9), 1144–1150 (2012).
42. N. A. Naderi, M. Pochet, F. Grillot, N. B. Terry, V. Kovanis, and L. F. Lester, "Modeling the injection-locked behavior of a quantum dash semiconductor laser," IEEE J. Sel. Top. Quantum Electron. **15**(3), 563–571 (2009).
43. X.-G. Wang, B.-B. Zhao, F. Grillot, and C. Wang, "Frequency noise suppression of optical injection-locked quantum cascade lasers," Opt. Express **26**(12), 15167–15176 (2018).
44. J. Duan, H. Huang, D. Jung, Z. Zhang, J. Norman, J. Bowers, and F. Grillot, "Semiconductor quantum dot lasers epitaxially grown on silicon with low linewidth enhancement factor," Appl. Phys. Lett. **112**(25), 251111 (2018).
45. N. Li, H. Susanto, B. Cemlyn, I. Henning, and M. Adams, "Nonlinear dynamics of solitary and optically injected two-element laser arrays with four different waveguide structures: a numerical study," Opt. Express **26**(4), 4751–4765 (2018).
46. X.-G. Wang, F. Grillot, and C. Wang, "Rate equation modeling of the frequency noise and the intrinsic spectral linewidth in quantum cascade lasers," Opt. Express **26**(3), 2325–2334 (2018).